

Article

Experimental Investigation of Phase Change Material-Based Battery Pack Performance Under Elevated Ambient Temperature

Mohammad J. Ganji , **Martin Agelin-Chaab** *  and **Marc A. Rosen** 

Faculty of Engineering and Applied Science, Ontario Tech University, Oshawa, ON L1G 0C5, Canada; mohammadjavad.ganji@ontariotechu.ca (M.J.G.); marc.rosen@ontariotechu.ca (M.A.R.)

* Correspondence: martin.agelin-chaab@ontariotechu.ca

Abstract: This study experimentally assesses the thermal performance of a proposed phase change material (PCM)-based battery pack under elevated ambient temperatures. In addition, the novel approach of the research addresses scenarios where the ambient temperature reaches the PCM's melting point while maintaining the initial temperature at the ideal operating point of 22 °C. The experiments employed nine 2500 mAh 18650 lithium-ion cells connected in series and subjected to constant-current discharges of 1C and 3C, with a conventional air-cooled system as the baseline and paraffin as the PCM. The results indicate that as the ambient temperature reached the PCM's melting point, approximately 98% utilization of the PCM around the heating cell was achieved. Additionally, the PCM demonstrates noticeable advantages over the baseline by stabilizing the temperature profile and reducing the maximum temperature increase rate from over 18 °C in the baseline system to around 7 °C. Notably, under a high-load (3C) discharge rate, the PCM-based system successfully maintained battery temperatures below 42 °C, demonstrating its effectiveness under demanding operational scenarios. These findings establish a critical baseline for PCM-based BTMSs operating under elevated ambient temperatures and up to the melting point of the PCM, thereby informing future research and development of more efficient PCM-based thermal management solutions.



Academic Editors: Jinsheng Xiao, Hengyun Zhang and Tianqi Yang

Received: 13 January 2025

Revised: 4 February 2025

Accepted: 4 February 2025

Published: 8 February 2025

Citation: Ganji, M.J.; Agelin-Chaab, M.; Rosen, M.A. Experimental Investigation of Phase Change Material-Based Battery Pack Performance Under Elevated Ambient Temperature. *Batteries* **2025**, *11*, 67. <https://doi.org/10.3390/batteries11020067>

Copyright: © 2025 by the authors. Licensee MDPI, Basel, Switzerland. This article is an open access article distributed under the terms and conditions of the Creative Commons Attribution (CC BY) license (<https://creativecommons.org/licenses/by/4.0/>).

1. Introduction

Lithium-ion batteries (LIBs) have emerged as the dominant energy storage solution for electric and hybrid vehicles due to their high specific energy, extended life cycle, and low self-discharge rates [1,2]. However, heat generation during charging and, more critically, during discharging poses significant safety risks and limits their effectiveness. Elevated temperatures can lead to thermal runaway, capacity degradation, and even fires, especially when the operational temperature exceeds the optimal range of 20 to 40 °C [3,4]. Uneven temperature distribution and inadequate thermal dissipation within battery packs further diminish LIB performance and efficiency.

To address these challenges, recent advancements in battery thermal management systems (BTMSs) aim to reduce maximum temperatures and achieve uniform temperature distribution while minimizing cooling energy consumption [5–8]. BTMSs are typically classified as active or passive based on their energy requirements. Active cooling utilizes external energy sources to dissipate heat through heat exchangers. At the same time, passive methods, such as phase change materials (PCMs), rely on natural heat transfer

mechanisms without external energy input [9–11]. Although passive methods are generally simpler, lighter, and more cost-effective, their applications are constrained by their thermal performance, especially under varying ambient temperatures.

Ambient temperature, referred to as inlet coolant temperature, can vary significantly due to factors such as geographic location, time of day, or cooling system failures, potentially raising the ambient temperature above the standard room temperature of 23 °C. The thermal performance of the PCMs quantified in this study as the temperature difference between cases with and without PCMs (Equation (3)) exhibits significant sensitivity to variations in ambient temperature [12]. Landini et al. [12] reported that PCMs may exhibit limitations under extreme operational conditions of LIBs, such as high ambient temperatures and high discharge rates. However, the current study focuses on assessing the PCM's capabilities under highly demanding conditions, where active cooling becomes unfavorable and heats up the system rather than dissipating the heat. Under these conditions, the PCM must utilize its stored energy to mitigate both the heat generated within the cells and the elevated ambient temperature affecting the cooling air ducts.

Extensive research has been conducted on PCM-based BTMSs as a primary cooling option for battery packs [13–16]. During phase transitions, PCMs can maintain a constant temperature profile until fully melted, which helps keep battery temperatures within safe limits. This provides extensive energy storage at the safe threshold of batteries, keeping the batteries below the melting point to ensure safety in high operational conditions. However, unfavorable cooling systems could hinder this effectiveness and affect the safety of batteries. Several studies have focused on optimizing PCM placement and enhancing heat dissipation through design modifications. Suo et al. [17] evaluated different PCM placements in prismatic battery modules combined with air cooling, finding that an optimized configuration reduced PCM volume significantly with minimal impact on temperature reduction. Dey et al. [18] investigated various fin designs in a cylindrical PCM-based BTMS, demonstrating that optimal fin configurations could maintain maximum temperatures under critical limits even at high discharge rates and simulated short circuit conditions with a resistance of 0.5 Ω.

Other researchers have introduced novel designs to improve thermal performance. Zhang et al. [19] developed new branch fin designs coupled with PCMs around a single battery module, while Khaboshan et al. [20] examined the efficacy of combining PCMs with metal foam and fins. Their findings indicated that integrating metal foam with PCMs substantially enhanced melting time and temperature uniformity. Sharma et al. [21] assessed fin designs combined with PCMs under high ambient temperatures, achieving superior cooling efficiency and preventing the PCM from melting during multiple charge/discharge cycles.

The effectiveness of composite PCMs (CPCMs) has also been explored. Wang et al. [22] evaluated a CPCM in a battery pack under various initial and ambient temperatures, finding that temperature control improved with higher ambient temperatures and discharge rates. Li et al. [23] implemented a novel passive thermal regulator based on PCMs, demonstrating an automatic natural thermal regulation mechanism that enhanced heat dissipation as temperatures rose. Wu et al. [24] introduced a flexible CPCM to maximize contact surface area with cylindrical cells, reducing maximum temperatures and ensuring better operating flexibility.

Integrating active cooling methods with PCM-based BTMSs has been shown to further improve thermal performance. Luo et al. [25] evaluated snowflake fins with liquid channels in a PCM-based cylindrical BTMS, achieving significant reductions in maximum temperature and improved temperature uniformity under high ambient temperatures and discharge rates. Xie et al. [26] incorporated micro-heat pipe arrays into a PCM-based BTMS, resulting in enhanced cooling performance and energy density.

Chen et al. [27] developed forked flow cooling channels in conjunction with a PCM-fin-based BTMS, identifying optimal configurations that balanced thermal performance and cooling power consumption. Zheng et al. [28] proposed a two-way wavy cooling plate coupled with a PCM-based BTMS, finding that certain flow direction strategies improved temperature uniformity without significantly increasing flow rates.

Shahid et al. [29] introduced a novel hybrid BTMS using stationary water channels and circulating air duct cooling integration with PCMs, which are in direct contact with the battery cells. The results revealed that the battery surface temperature reached the PCM melting temperature after the fifth discharge cycle. Moreover, after the seventh cycle, the temperature uniformity started to change as the PCM melting percentage exceeded 2.3%. In another study [30], the authors replaced water channels with cold plates. The results revealed that using cold plates instead of water channels decreased the maximum temperature by 1.5 °C, preventing the PCM from reaching its melting temperature. Also, maximum temperature uniformity was reduced from 3.2 °C to 1.2 °C. Further investigations [31] showed that increasing the height of the air duct and Reynolds number by more than 6 mm and 1950, respectively, does not significantly improve cooling performance. The present study experimentally examines the thermal performance using a similar air duct and water channels but without any water in the proposed BTMS. Natural air circulation is proposed instead of stationary water inside the cylindrical channels due to battery safety measures and simplicity.

The comprehensive review and experimental insights underscore the critical role of thermal management in enhancing the safety, performance, and lifespan of LIBs, particularly under varying operational conditions. Ambient operating temperatures can elevate significantly due to cooling system failures, and such elevated temperature conditions can consequently affect the thermal performance of PCMs and BTMSs, potentially compromising battery safety and efficiency. Despite prior advancements in PCM-based BTMSs, the existing literature has a limited scope of performance of ambient temperatures up to 30 °C.

The present study aims to address this gap by experimentally evaluating the effectiveness of a PCM-based BTMS at elevated ambient temperatures up to 42 °C, which is beyond what currently exists in the literature. Additionally, the study extends the evaluation of the elevated ambient temperature up to the melting point of the PCM to provide new insights into PCM performance under its operational limit. Thus far, no study has evaluated the performance of the PCM at its melting point temperature. Furthermore, the study aims to maintain the initial temperature at an ideal operating point of 22 °C for all tested experiments to ensure a consistent starting behavior of the PCM during the experiments. The rationale is to replicate scenarios in which a cooling system fails or, if there are any other contributing factors, leads to heating the system rather than dissipating heat. Consequently, this also allows for the assessment of the material's capacity for stored latent heat and regulates the maximum battery temperature at both low and high discharge rates and under both favorable and unfavorable cooling conditions (i.e., 22–42 °C ambient temperature). Furthermore, the study quantifies the degree of PCM melting and assesses how effectively stored energy is utilized to mitigate ambient temperature rise. By analyzing the effects of elevated ambient temperatures and PCMs' latent heat utilization, this research provides valuable insights into the thermal management of LIBs under varying operational conditions. The findings are expected to provide a baseline for PCM-based BTMSs under elevated ambient temperatures for future research and the development of more efficient thermal management solutions.

2. Methodology

2.1. Experimental Setup

Nine cylindrical lithium-ion Samsung INR18650-25R batteries were utilized. Each battery had a capacity of 2500 mAh and a nominal voltage of 3.7 V. The batteries were arranged in series within a cuboid battery pack, with each battery spaced 6 mm apart to maintain consistency with previous research by Shahid et al. [29]. The battery pack was constructed using a medium-density fiberboard (MDF) with a thickness of 6.5 mm, assembled and sealed with high-temperature-resistant sealant glue. MDF was selected for its availability and suitability for precise laser cutting. The internal dimensions of the battery pack were 7.5 cm in width and 5.5 cm in height, accommodating the INR18650-25R batteries (18 mm diameter, 65 mm height). An isometric visualization of the battery pack is presented in Figure 1a.

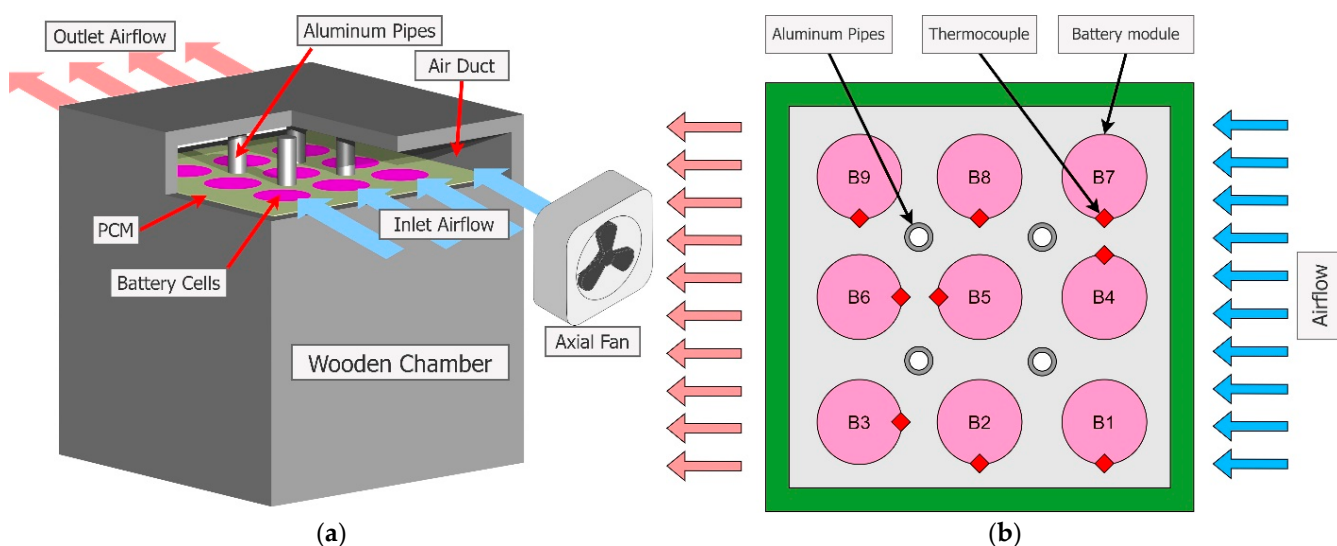


Figure 1. (a) Isometric view of the battery pack configuration for Phase 1, and (b) top view of the battery pack showing the thermocouple placement.

The batteries were interconnected using nickel strips measuring 5 mm in width, 4 cm in length, and 0.5 mm in thickness. Four vertical air pipes with an outer diameter of 6 mm and a wall thickness of 1 mm were installed between the battery cells to facilitate heat dissipation. These air pipes were strategically placed to ensure efficient heat dissipation from the battery cells, thereby maintaining the desired operating temperature. The chosen air pipe geometry was selected based on its consistency with previous research, as well as its symmetry, simplicity, and ease of assembly, in contrast to more complex rectangular or irregular geometries. Aluminum was used for the air pipes. An air duct, matching the length and width of the battery chamber and with a height of 1.9 cm, was placed above the battery pack to dissipate heat from the air pipes. An axial AC fan (GDSTIME 1203) was employed to ensure steady airflow through the duct, achieving an inlet speed of 2.1 ± 0.1 m/s, as measured by a Proster anemometer. The inlet air temperature was controlled using a 227 L (8 cubic feet) thermal chamber (SD-508, Associated Environmental Systems) with an accuracy of ± 0.5 °C. The walls of the battery pack were assumed to be adiabatic, implying that all heat dissipation relied exclusively on the air duct. Real images of the thermal chamber and the experimental setup installed inside it are shown in Figure 2.

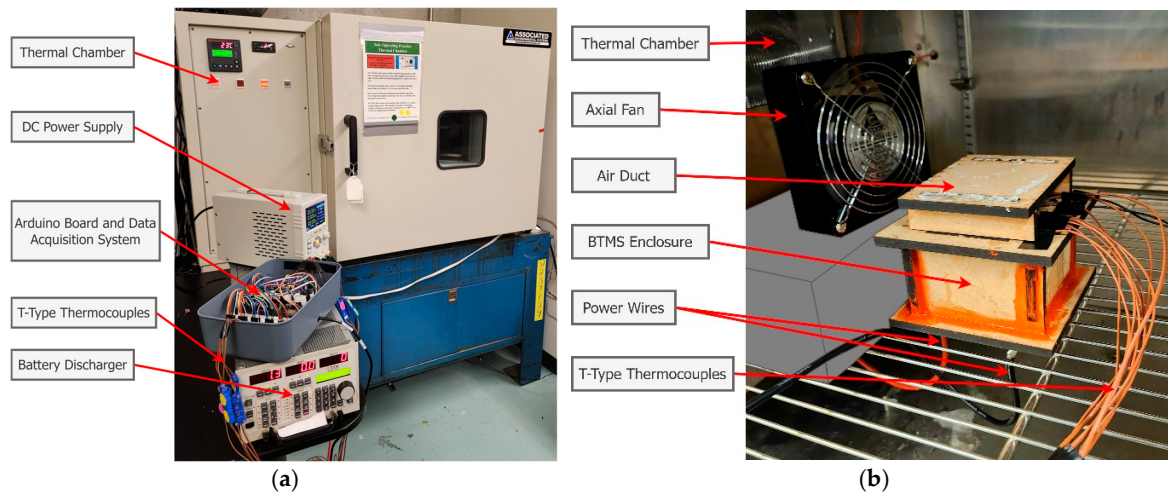


Figure 2. (a) Real image of the experimental equipment, and (b) real image of the experimental setup installed inside the thermal chamber.

T-type thermocouples (5TC-TT-T-24-72 Omega), with a reported accuracy of ± 0.5 °C, were installed to monitor the temperature distribution within the battery pack. Nine thermocouples were attached to the surface of the batteries at the center of the total height, capturing temperature data from all sides of the batteries, as depicted in Figure 1b. Each thermocouple was connected to an Adafruit 3263 temperature sensor (± 0.075 °C reported accuracy) and interfaced with an Arduino Mega microcontroller (Elegoo MEGA 2560 R3). The temperature readings were transmitted to a computer via the Arduino terminal connection for real-time monitoring and data logging. A schematic of the data acquisition and electrical setup is provided in Figure 3.

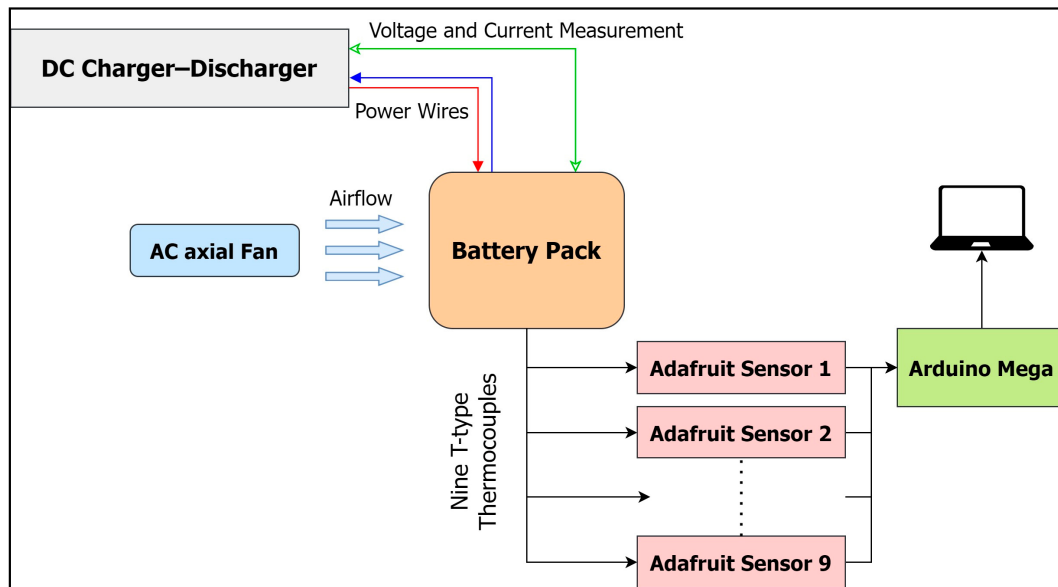


Figure 3. Schematic of the data acquisition and electrical setup.

Paraffin wax, with a melting temperature range of 40–42 °C, was selected as the working PCM. Despite its flammability, paraffin offers an optimal balance of cost, thermal storage capacity, chemical stability, and availability across various melting points. The flammability concern can be mitigated later through appropriate system design and encapsulation. While the optimal temperature range for many lithium-ion cells is typically 30–35 °C, the batteries are designed to withstand operating temperatures of up to 40 °C.

Consequently, paraffin 40–42 °C was chosen to maintain battery temperatures below this point. Paraffin with a lower melting point was deemed unsuitable, as the scope of this research aims to simulate higher temperatures and test the batteries up to their safe threshold of 40 °C. The manufacturer's temperature specifications for the PCM were validated through multiple thermal experiments conducted before and after the study to ensure its thermophysical stability. The corresponding average results of the melting experiments are presented in Figure 4, illustrating the melting and solidification temperature profiles of the paraffin 40–42 PCM, confirming a melting temperature of 41 ± 1 °C. To improve comparative visualization, the x-axis has been normalized in time. As anticipated, the solidification process takes approximately twice as long as the melting process. The physical properties of the materials used in this study are provided in Table 1. Based on the dimensions of the battery pack and the available volume for PCM storage, 177 ± 1 mL of molten paraffin was poured into the battery pack, corresponding to 136 ± 1 g of material. The volume of the PCM was measured using a precise graduated syringe, with repeated measurements ensuring consistency and accuracy.

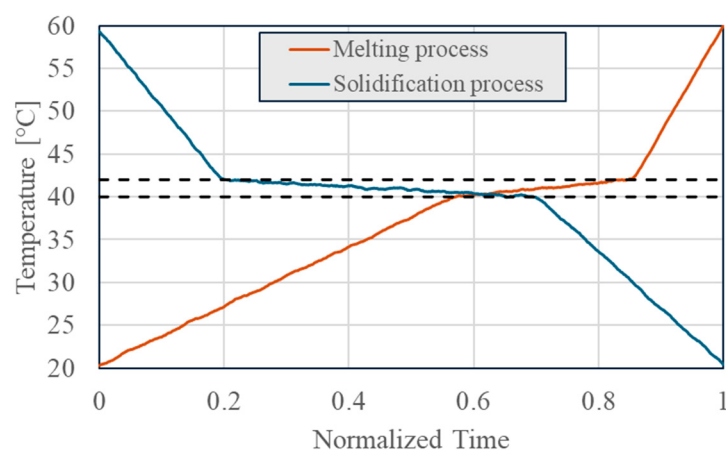


Figure 4. Paraffin 40–42 PCM temperature profiles of melting and solidification (time axis is normalized for better visualization of the temperature profile).

Table 1. Physical properties of materials used in experiment *.

Property	Unit	Wood [31]	Aluminum [31]	Nickel [32]	PCM (Solid–Liquid) ** [33]	Air [31]
Specific Heat at Constant Pressure (C_p)	J/kg · K	2310	871	444	2150–2250	1006
Thermal Conductivity (k)	W/m · K	0.173	202.4	90.9	0.21–0.18	0.026
Density (ρ)	kg/m ³	700	2719	8908	880–770	1.225
Latent Heat of Fusion (L_f)	kJ/kg	-	-	-	245	-
Liquidus Temperature (T_l)	°C	-	-	-	42	-
Solidus Temperature (T_s)	°C	-	-	-	39	-
Electrical Resistivity (ρ_e)	Ω · m	-	2.65×10^{-8} [32]	6.84×10^{-8}	-	-

* The physical properties provided are measured at 25 °C and 1 bar [31–33]. ** The PCM used in this study is 40–42 paraffin wax.

2.2. Experimental Procedure

The battery pack was installed inside the thermal chamber, where the ambient temperature within the chamber was controlled with an accuracy of ± 0.5 °C. The initial temperature of the battery pack was maintained at 22 ± 0.1 °C for all experiments. Consequently, variations in ambient temperature only affected the air duct flow temperature. Five ambient temperatures were studied, ranging from 22 °C to 42 °C in increments of 5 °C.

The batteries were configured in a series arrangement and initially charged using a constant current (CC) of 4 ± 0.01 A until the overall voltage reached a cutoff of 37.8 ± 0.005 V, corresponding to 4.2 V per cell, using the DC Power Supply OWON SP6103 with specified accuracy. Subsequently, the charging process continued with a constant voltage (CV) of

37.8 ± 0.005 V until the charging current decreased to 0.1 ± 0.01 A, defined as the cutoff current according to the manufacturer's specifications.

For the discharging procedure, the series-connected batteries were subjected to constant current discharges at rates of 1C and 3C, corresponding to currents of 2.5 ± 0.01 A and 7.5 ± 0.01 A, respectively, using the Multifunctional Load TDI RBL488 with specified accuracy. The discharge process continued until the total voltage dropped to 22.5 ± 0.01 V, corresponding to 2.5 V per cell. Thereafter, discharging proceeded with a constant voltage of 22.5 ± 0.01 V until the discharge current fell to 0.1 A, designated as the cutoff current per the manufacturer's specifications. The discharge power usage profiles of the battery modules during the experiments are illustrated in Figure 5, where the horizontal axis is normalized by the total discharge times to facilitate better comparison between different discharge rates. The total discharge times for 1C and 3C discharge rates are approximately 66 min and 25 min, respectively.

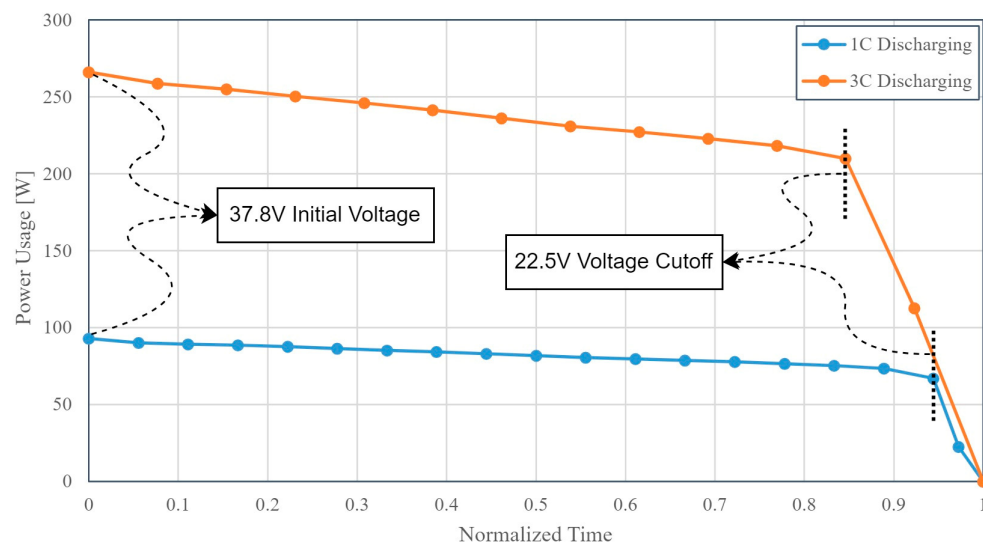


Figure 5. Discharge power usage profile of the battery modules.

2.3. Consistency and Uncertainty Analysis

The methodology proposed by Moffat (1988) [34] was employed to quantify the uncertainties associated with the experimental results. In this study, two primary sources of uncertainty were identified: bias error and precision error. Bias errors represent systematic deviations inherent to the measurement system, while precision errors represent random fluctuations observed during repeated measurements. Both types of errors were quantified to ensure the reliability of the experimental results.

The bias error originates from the measurement instruments used in the experiments. In this case, thermocouples and Adafruit sensors were employed for temperature measurements. According to the manufacturers' specifications, the thermocouples have an accuracy of ± 0.5 °C (δT_{TC}), while the Adafruit sensors have an accuracy of ± 0.075 °C (δT_S). Since both devices were used in series, their combined uncertainty was calculated using the RSS method [35]:

$$\text{Absolute Bias Error } (\text{°C}) \delta T = \sqrt{(\delta T_{TC})^2 + (\delta T_S)^2} \approx 0.5056 \text{ °C} \quad (1)$$

The resulting absolute bias error for the temperature measurements was determined to be ± 0.5056 °C, which is consistent across all experimental conditions, as the bias error depends solely on the instrumentation.

The precision error was assessed based on the variability of the repeated temperature measurements. Precision error is quantified using the maximum discrepancy of data from the mean value, expressed in the same unit as the measurement. The maximum discrepancy is the largest deviation observed between an individual measurement and the mean value of the repeated data for each experiment. This measure provides a straightforward representation of the worst-case scenario for the absolute precision error.

Each experiment was repeated multiple times according to the discharge power usage shown in Figure 5. Figure 6 presents the maximum temperature deviations from the mean values, referred to as the absolute precision error, for each tested condition. The results indicate a maximum absolute precision error of $\pm 0.29^{\circ}\text{C}$, highlighting the consistency of the experimental data.

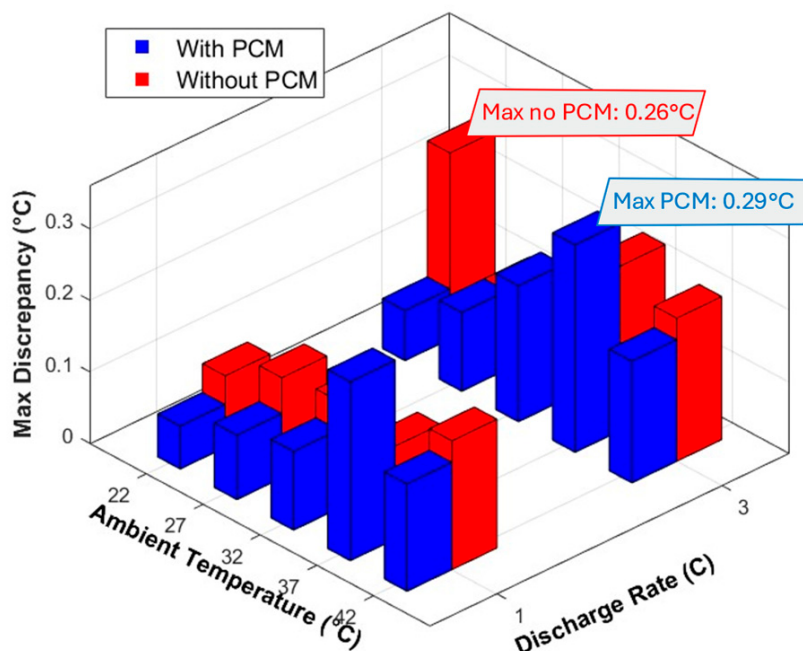


Figure 6. Maximum temperature deviation from the average in repeated experiments.

The total uncertainty of the measurements was determined by combining the relative bias error and the relative precision error using the RSS method:

$$\text{Total Uncertainty (\%)} = \sqrt{(\text{Relative Bias Error})^2 + (\text{Relative Precision Error})^2} \quad (2)$$

The results are summarized in Table 2 for the minimum and maximum temperatures measured in the experiment. The table highlights the bias error, maximum precision error, and maximum total uncertainty.

Table 2. Errors and total uncertainty of the experiments.

Parameters	Reference Value	Absolute Bias Error ($^{\circ}\text{C}$)	Relative Bias Error (%)	Max Absolute Precision Error ($^{\circ}\text{C}$)	Max Relative Precision Error (%)	Max Total Uncertainty (%)
Min. Temperature	20 $^{\circ}\text{C}$	± 0.5056	2.53	± 0.29	1.45	2.91
Max. Temperature	55 $^{\circ}\text{C}$	± 0.5056	0.92	± 0.29	0.52	1.06

The combined analysis of bias error, precision error, and total uncertainty ensures the reliability and accuracy of the experimental results, providing the validity of the measurements and the overall experimental methodology.

3. Results and Discussion

3.1. Temperature Uniformity Analysis

The surface temperature of all nine battery cells in distinct orientations was measured using nine thermocouples attached to the center of each battery, as depicted in Figure 1b. The thermocouples were strategically positioned to capture a comprehensive range of orientations, including facing the outer wall parallel and perpendicular to the inlet flow, facing the center of the chamber, and being adjacent to others. Each orientation was accurately monitored by a corresponding thermocouple. Figure 7 illustrates the temperature data for the baseline 1C discharge rate at an ambient temperature of 22 °C. The figure reveals that all recorded temperatures exhibit a variance of less than 0.1 °C. This value is below the estimated inherent experimental error in the measurement, demonstrating a high degree of temperature uniformity across the batteries. This consistent behavior was observed in other experiments as well across all tested ambient temperatures. Accordingly, only the temperature measured by thermocouple T1 will be presented and analyzed in subsequent analyses; any reference to temperature henceforth specifically pertains to T1 measurements.

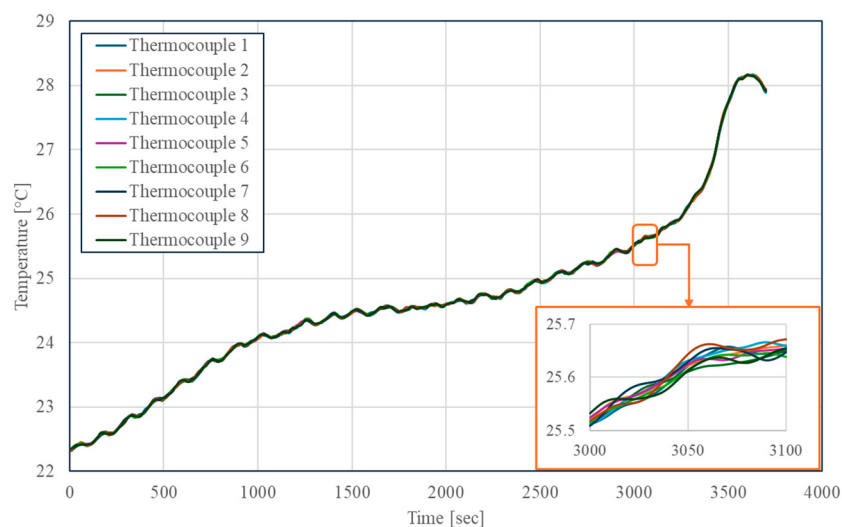


Figure 7. Temperature uniformity analysis across installed thermocouples.

3.2. Temperature Analysis

Figure 8a,b presents the temperature profiles of the batteries, as measured by Thermocouple 1, during the discharge period at 1C and 3C rates, respectively, with and without the PCM under various ambient temperatures. For ease of comparison, both figures are normalized by 3700 and 1400 s, respectively. At a 1C discharge rate and ambient temperatures of 22 °C and 27 °C, incorporating the PCM has minimal impact on both the temperature profile and the maximum temperature, showing the underutilization of current PCM under a 1C discharge rate and favorable ambient temperatures. This result stems from the ambient temperatures being significantly lower than the PCM's melting point (40–42 °C), preventing it from undergoing phase change and utilizing its latent heat absorption capabilities.

However, at higher ambient temperatures of 32 °C and 37 °C, the PCM effectively reduces the rate of temperature rise during discharge, lowering the maximum temperature by approximately 2.5 °C and 2.1 °C, respectively. Moreover, the effect of the PCM is even more pronounced at an ambient temperature of 42 °C, achieving a thermal performance comparable to the baseline condition at 37 °C without a PCM. This indicates that the PCM becomes more effective as the system temperature nears its melting point.

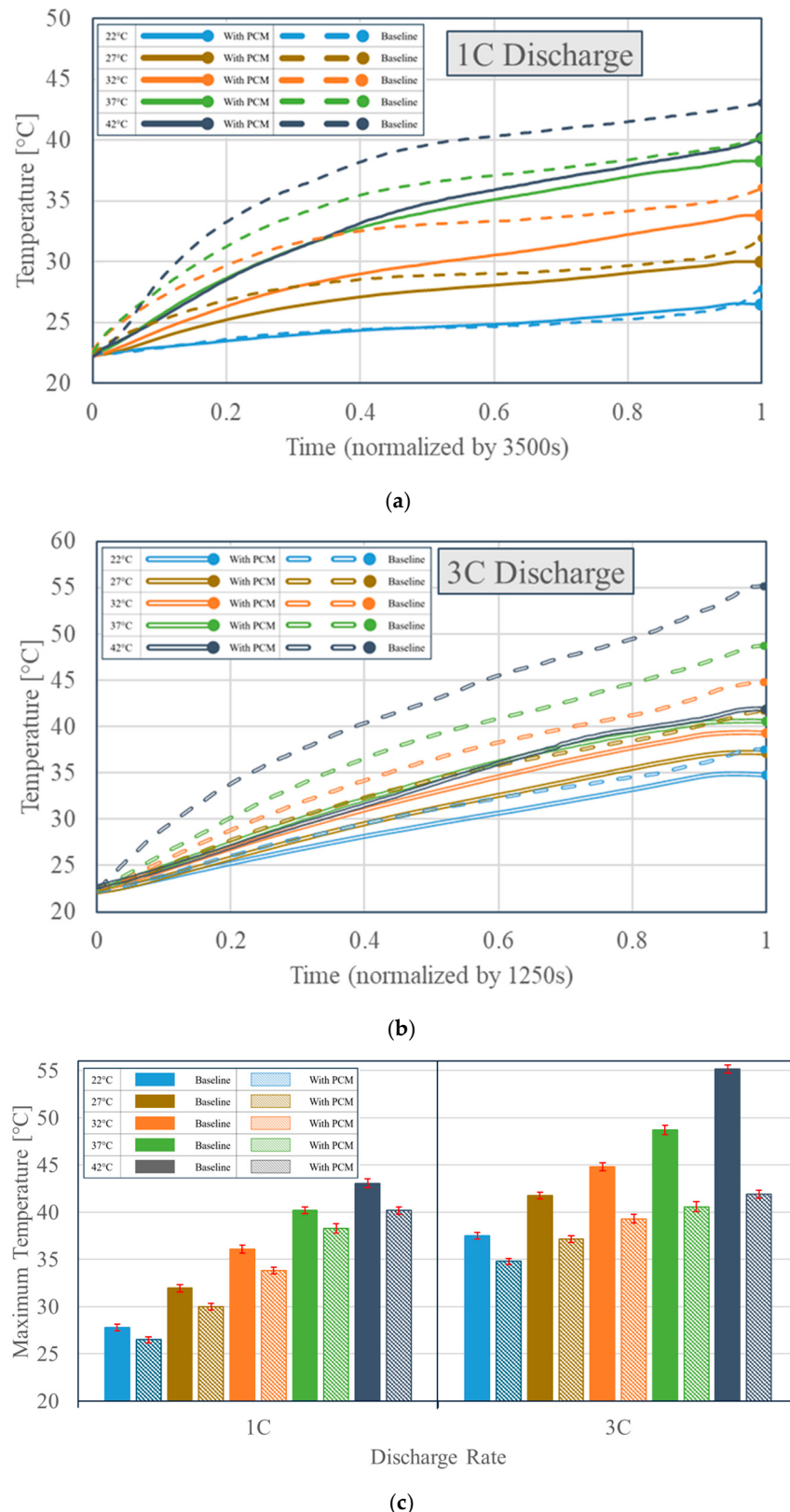


Figure 8. Temperature profile of batteries during constant current discharge at (a) 1C and (b) 3C, and (c) maximum temperature bar chart for each experiment.

As anticipated from the literature, the benefits of using PCMs are more evident at higher discharge rates. Nevertheless, there is a lack of comprehensive understanding of

how ambient temperatures approaching the melting point of the PCM affect performance under varying discharge rates, from normal levels (1C) to higher rates (3C).

At a discharge rate of 3C, employing the PCM significantly enhances thermal management, reducing the maximum temperature by approximately 2.6 to 13.3 °C across the tested ambient temperatures. In contrast, under a 1C discharge rate, the maximum temperature was notably decreased by values ranging from 1.6 to 2.5 °C. This underscores the PCM's increased efficacy at higher discharge rates, which generate greater heat and accelerate the PCM's latent heat activation.

Figure 8b shows that with the implementation of the PCM, the maximum temperature remained below 42 °C, which is the melting temperature of the PCM. However, at 27 °C, where the PCM did not reach its melting point, the maximum temperature was reduced by 4.5 °C, which is double the reduction compared to the same ambient temperature at a 1C discharge rate. Additionally, the PCM usage at a 3C discharge rate with a higher ambient temperature (e.g., 42 °C, 37 °C, or 32 °C) exhibits similar cooling performance to the case without the PCM at an ambient temperature of 27 °C. For example, in Figure 8b, the temperature profile at 42 °C with the PCM and at 27 °C without the PCM are identical.

Figure 8c presents the maximum battery temperature measured under each experimental condition, with error bars indicating measurement uncertainties. The data show that, in the absence of a PCM, increases in ambient temperature led to a nearly constant upward trend in the maximum temperature for both the 1C and 3C discharge cases. By contrast, integrating PCM substantially moderates this temperature rise, especially once the system reaches the PCM's melting range. This mitigating effect becomes more pronounced at higher discharge rates, where the batteries generate enough heat to activate the PCM's latent heat storage capacity. Consequently, the maximum temperatures in PCM-equipped setups remain comparatively lower, underscoring the PCM's effectiveness in stabilizing thermal behavior under demanding operational conditions.

3.3. PCM Performance Analysis

Hybrid cooling systems are employed to dissipate heat from batteries and to maintain the maximum temperature below the PCM's melting point. Although incorporating a PCM reduces the equivalent thermal conductivity between the cells and the environment, it provides latent cooling energy storage that becomes active at the PCM's melting point, thereby preventing system overheating [1,36,37]. During the discharge period, the battery cells are assumed to produce a consistent heat flux profile according to the discharge rates. Given the consistent cooling properties, the equivalent thermal conductivity can also be considered constant [38]. Consequently, variations in ambient temperature primarily impact the rate at which the PCM releases stored energy, thereby affecting the system's thermal performance.

Figure 9 presents the temperature reduction performance of the PCM under different ambient temperatures for both 1C and 3C discharge rates. The cooling performance is quantified by comparing the temperature reduction to the baseline case without a PCM, as defined by Equation (3). To assess the PCM's performance per unit of energy stored and account for its dependence on the quantity inside the pack, Equation (3) has been normalized by the PCM's latent heat of fusion (L_f) and its mass (m_{PCM}).

$$\text{PCM Performance } [\text{°C}/\text{kJ}] = \frac{T_{\text{without PCM}} - T_{\text{with PCM}}}{L_f \cdot m_{PCM}} \quad (3)$$

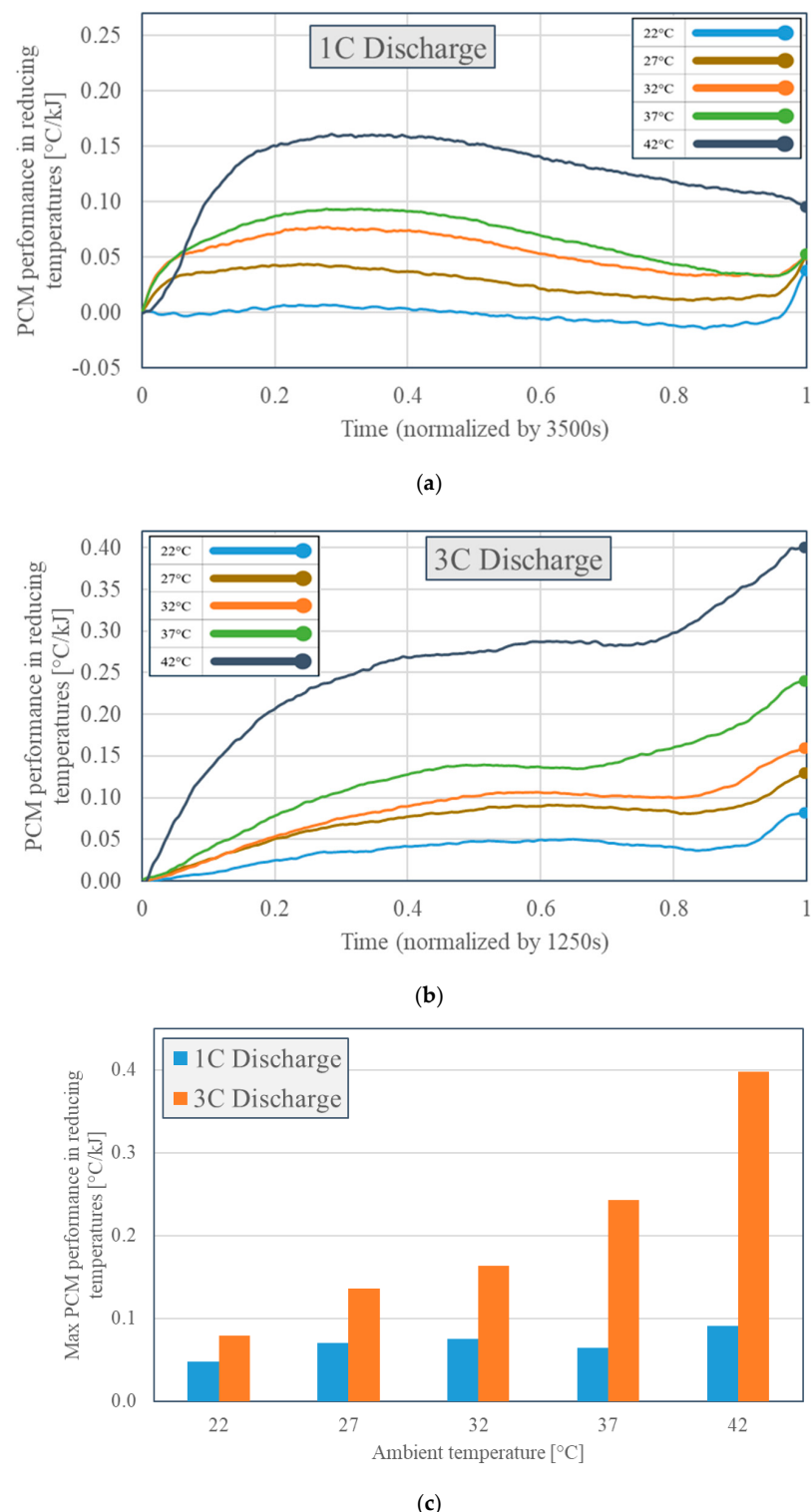


Figure 9. PCM performance in reducing temperatures under elevated ambient temperatures at (a) 1C and (b) 3C discharge rates and (c) maximum attribution of PCM in reducing temperature.

Figure 9a demonstrates the PCM performance at a 1C discharge rate for various ambient temperatures. At 22 °C, the PCM shows a minimal or even negative effect in the early stages of the discharge. This is because the ambient temperature is well below the PCM's melting point (40–42 °C), preventing the utilization of latent heat absorption. However, towards the later stages of the discharge, the PCM starts to show positive cooling effects. This late improvement in performance can likely be attributed to the sensible heat

storage of the PCM rather than latent heat absorption, as the system temperature remains below the melting point of the PCM. The PCM proves more effective for higher ambient temperatures as the system temperature approaches its melting point. However, even in these cases, the maximum temperatures during the experiment remain below the melting point of 40–42 °C, except for the cases of 37 °C and 42 °C ambient temperatures. For these two conditions, the maximum temperatures reach 38.2 °C and 40.3 °C, respectively, still slightly below the melting point of the PCM. Therefore, the cooling effect observed at the higher ambient temperatures of 27 °C, 32 °C, and 37 °C is largely influenced by the sensible heat storage. Only at 42 °C does the PCM utilize its latent heat capacity, where a significant reduction of up to 5 °C is achieved before the difference diminishes as the thermal management system reaches the ambient temperature during the second half of the experiment. Consequently, the current PCM has been underutilized under the 1C discharge rate since the maximum achieved temperature is below the melting point, and no latent heat absorption occurred at these conditions. If further reduction or stricter regulation of the maximum temperature is necessary under these conditions, a PCM with a lower melting point can be considered.

In contrast to the 1C discharge, the higher heat generation in the 3C discharge activates the PCM melting more rapidly, resulting in noticeable cooling effects early in the experiment, as illustrated in Figure 9b. At lower ambient temperatures, the PCM performance is driven primarily by sensible heat absorption since the system temperatures do not reach the melting range of the PCM. Despite this, the PCM still provides a consistent reduction in temperature throughout the discharge. As the ambient temperature increases, the system temperature approaches the PCM's melting range, leading to partial phase change and the activation of both sensible and latent heat absorption. This results in a more pronounced cooling effect as the PCM transitions into its melting phase. At the highest ambient temperature, nearly the entire PCM undergoes a phase change, maximizing its cooling potential. However, as with the 1C discharge case, the cooling effectiveness of the PCM over the case without the PCM diminishes over time due to the better utilization of traditional cooling rather than the latent capacity in the case without the PCM, indicating a limit to sustained performance.

Figure 9c illustrates the comparison of maximum PCM performance for both 1C and 3C discharge rates across varying ambient temperatures. As the ambient temperature increases, the cooling performance improves for both rates, with the 3C discharge consistently showing greater reductions due to higher heat generation and faster starting of PCM phase change. At lower ambient temperatures, the cooling effect is primarily due to sensible heat absorption. In comparison, latent heat absorption significantly enhances performance at higher temperatures as the system approaches the PCM's melting range. The results highlight the dependence of PCM efficiency on the discharge rate and ambient temperature, with the 3C discharge achieving the most substantial reductions.

3.4. PCM Phase Change Analysis

The benefits of using a PCM at high discharge rates and elevated ambient temperatures stem from harnessing the PCM's stored latent energy, which helps stabilize temperatures during the phase change process. Analyzing the melting percentage at the end of discharge is essential to understanding how effectively the PCM is utilized in the system. According to the literature [20], the simplified melting percentage of the PCM in an elemental volume is calculated as follows:

$$\text{PCM Melting Percentage} = \begin{cases} 0 & \text{if } T_m < T_s \\ \frac{T_m - T_s}{T_l - T_s} & \text{if } T_s < T_m < T_l \\ 1 & \text{if } T_m > T_l \end{cases} \quad (4)$$

Here, T_m , T_l , and T_s denote the maximum temperature, PCM liquidus temperature, and PCM solidus temperature, respectively. The quantified value of the PCM melting percentage does not equate to the total melting fraction of the PCM contained within the chamber. Rather, it pertains specifically to the controlled volume surrounding the measuring thermocouple. Table 3 presents the PCM melting percentages at the end of the experiments. During the 1C discharge experiments, no PCM melted at an ambient temperature below the melting point, indicating that latent heat was not utilized under these conditions. However, during the 3C discharge experiments, the PCM melting commenced at an ambient temperature of 32 °C, with 12.4% of the PCM melting, and reached nearly complete utilization at 42 °C, with approximately 98% of the PCM melting.

Table 3. PCM melting percentage (in %) at the end of experiments.

Ambient Temperature (T_m) [°C]	1C Discharge Rate	3C Discharge Rate
22	0	0
27	0	0
32	0	12.4
37	0	54.3
42	46.3	97.6

Additionally, considering the 3C discharge rate, the interpolation of Figure 9 and the melting percentage data indicate that the PCM started contributing its stored cooling capacity (i.e., latent heat) to the system after achieving a 4.6 °C reduction in maximum temperature. Figure 10 illustrates the corresponding interpolation analysis. The second-degree polynomial interpolation analysis yielded R-squared values of 0.9981. From this analysis, it can be inferred that the maximum utilization of PCM at a 3C discharge rate (i.e., 100% melting) corresponds to a PCM performance of approximately 13.6 °C in maximum temperature reduction. Note that the formula derived from the 3C discharge rate results cannot be applied to the 1C analysis. Furthermore, the PCM melting percentage, as described in Equation (3), pertains solely to the close proximity of the thermocouple probes and should not be interpreted as the total melting fraction.

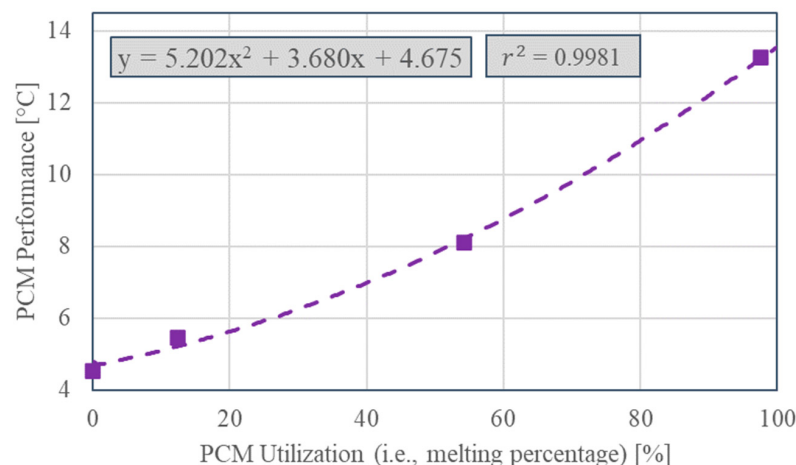


Figure 10. Interpolated PCM utilization and corresponding cooling performance in terms of maximum temperature reduction at a 3C discharge rate.

In summary, the findings demonstrate the effectiveness of the PCM in mitigating temperature rises and maintaining thermal stability within the battery pack under varied operational conditions. The PCM efficiently utilizes its stored latent heat to limit the maximum temperature, particularly at high ambient temperatures and discharge rates. While underutilized at a 1C discharge rate, it achieved a complete local phase transition at the 3C rate and an ambient temperature of 42 °C. Despite achieving excellent temperature

uniformity across the battery surfaces, with variations less than $0.1\text{ }^{\circ}\text{C}$, a key limitation was identified in the PCM's thermal behavior. Visual inspection revealed that only the PCM in close proximity to the battery surfaces—within approximately 1 mm—underwent phase change and melted. The PCM located farther from the batteries remained solid and was not utilized in the phase change process. This limitation is attributed to the inherently low thermal conductivity of paraffin, which restricts efficient heat transfer throughout the PCM volume. Consequently, only a fraction of the PCM's latent heat storage potential was utilized, thereby constraining its overall effectiveness under high thermal loads.

4. Conclusions

This study experimentally investigated the thermal performance of a proposed PCM-based battery pack under elevated ambient temperatures. In addition, the novel approach of the research addresses scenarios where the ambient temperature reaches the PCM's melting point while maintaining the initial temperature at the ideal operating point of $22\text{ }^{\circ}\text{C}$. The experiments employed nine 2500 mAh 18650 lithium-ion cells connected in series and subjected to constant-current discharges of 1C and 3C. A conventional air-cooled thermal management system served as the baseline, and paraffin with a melting temperature of $40\text{--}42\text{ }^{\circ}\text{C}$ was selected as the integrated PCM in the battery pack, including an inlet air speed of $2.1 \pm 0.1\text{ m/s}$ and $177 \pm 1\text{ mL}$ of paraffin. The novelty of this research lies in the experimental evaluation of the thermal efficiency of the PCM in responding to rising ambient temperatures, reaching the PCM's melting point by quantifying the percentage of PCM's local melting and its utilization of stored energy. The following conclusions were drawn:

- At ambient temperatures approaching the PCM's melting point, the local utilization percentage of the PCM reached approximately 98% around the batteries and air pipes. This indicates the near-complete engagement of the PCM around the heating sources. However, visual inspection revealed that the PCM was not contributing to its full capacity and left a portion of its volume unmelted. This necessitates the need for further enhancements of pure PCM systems in ambient temperatures exceeding the melting point to effectively manage elevated environmental conditions while fully leveraging the PCM's latent heat storage capacity for maintaining optimal battery temperatures.
- Using the PCM diminishes the impact of rising ambient temperatures on both the maximum battery temperature and the overall temperature profile. With the PCM, the maximum temperature varied by about $7 \pm 1\text{ }^{\circ}\text{C}$ across the tested temperature range, while the baseline system without a PCM exhibited fluctuations exceeding $18 \pm 1\text{ }^{\circ}\text{C}$. This underscores the PCM's effectiveness in stabilizing thermal performance despite rising external temperatures.
- During high-stress conditions, such as a 3C discharge rate under elevated ambient temperatures, the PCM became more suitable for thermal management. The maximum battery temperature remained below $42\text{ }^{\circ}\text{C}$ in the PCM-integrated system, whereas the baseline system experienced a significant temperature increase from $38\text{ }^{\circ}\text{C}$ to $55\text{ }^{\circ}\text{C}$. This demonstrates the PCM's effectiveness in ensuring thermal stability under demanding conditions.
- At a 1C discharge rate, the PCM achieved a modest maximum temperature reduction of up to $3.1\text{ }^{\circ}\text{C}$. However, at a 3C discharge rate, the PCM's performance improved considerably with rising ambient temperatures (from $22\text{ }^{\circ}\text{C}$ to $42\text{ }^{\circ}\text{C}$), reducing the maximum temperature by $2.6\text{ }^{\circ}\text{C}$ to $13.3\text{ }^{\circ}\text{C}$, respectively. This reinforces the PCM's enhanced thermal management capability under elevated operational and environmental stress levels.

These conclusions underscore the potential impact of using a PCM at elevated ambient temperatures, particularly under high discharge rates, on the thermal management of the battery packs. By examining ambient conditions up to the PCM's melting point and correlating local melting percentages with resulting temperature reductions, this research addresses a gap in the existing literature and provides a foundation for further advancements in PCM-based thermal management systems under a wider range of ambient operational conditions. The limitation of the study is the use of paraffin as the PCM since it is flammable. However, the flammability concern can be later mitigated through appropriate system design and packaging.

Author Contributions: Conceptualization, M.J.G., M.A.-C. and M.A.R.; methodology, M.J.G.; software, M.J.G.; validation, M.J.G., M.A.-C. and M.A.R.; formal analysis, M.J.G.; investigation, M.J.G.; resources, M.A.-C. and M.A.R.; data curation, M.J.G.; writing—original draft preparation, M.J.G.; writing—review and editing, M.J.G., M.A.-C. and M.A.R.; visualization, M.J.G.; supervision, M.A.-C. and M.A.R.; project administration, M.A.-C.; funding acquisition, M.A.-C. All authors have read and agreed to the published version of the manuscript.

Funding: This research was funded by the Natural Sciences and Engineering Research Council of Canada (NSERC), grant number RGPIN-2018-05369.

Data Availability Statement: The data presented in this study are available on request from the corresponding author due to confidentiality agreements.

Acknowledgments: The authors acknowledge with gratitude the financial support provided by the Natural Sciences and Engineering Research Council of Canada (especially the NSERC CREATE and NSERC Discovery Grant programs). The technical support of Seham Shahid, a recent graduate of Ontario Tech, is also greatly appreciated.

Conflicts of Interest: The authors declare no conflict of interest.

Nomenclature

C	Discharge rate (1/h)
C_p	Specific heat at constant pressure
k	Thermal conductivity (W/m·K)
L_f	Latent heat of fusion (kJ/kg)
T	Temperature (°C)
T_l	Liquidus temperature (°C)
T_s	Solidus temperature (°C)
Greek Symbols	
δT_S	Error of Adafruit sensor (°C)
δT_{TC}	Error of thermocouple (°C)
ρ	Density (kg/m ³)
ρ_e	Electrical resistivity (Ω·m)
Abbreviations and Acronyms	
BTMS	Battery Thermal Management System
CPCM	Composite Phase Change Material
CC	Constant Current
CV	Constant Voltage
C-rate	Current Rate
LIB	Lithium-Ion Battery
Li-ion	Lithium-Ion
MDF	Medium-Density Fiberboard
PCM	Phase Change Material

References

1. Luo, J.; Zou, D.; Wang, Y.; Wang, S.; Huang, L. Battery thermal management systems (BTMs) based on phase change material (PCM): A comprehensive review. *Chem. Eng. J.* **2022**, *430*, 132741. [[CrossRef](#)]
2. Shahid, S.; Agelin-Chaab, M. Experimental and numerical studies on air cooling and temperature uniformity in a battery pack. *Int. J. Energy Res.* **2018**, *42*, 2246–2262. [[CrossRef](#)]
3. Leng, F.; Tan, C.M.; Pecht, M. Effect of temperature on the aging rate of Li ion battery operating above room temperature. *Sci. Rep.* **2015**, *5*, 12967. [[CrossRef](#)] [[PubMed](#)]
4. Shahid, S.; Agelin-Chaab, M. A review of thermal runaway prevention and mitigation strategies for lithium-ion batteries. *Energy Convers. Manag.* **X** **2022**, *16*, 100310. [[CrossRef](#)]
5. Chen, K.; Wu, W.; Yuan, F.; Lin, C.; Wang, S. Cooling efficiency improvement of air-cooled battery thermal management system through designing the flow pattern. *Energy* **2019**, *167*, 781–790. [[CrossRef](#)]
6. Wang, M.; Teng, S.; Xi, H.; Li, Y. Cooling performance optimization of air-cooled battery thermal management system. *Appl. Therm. Eng.* **2021**, *195*, 117242. [[CrossRef](#)]
7. Wang, N.; Li, C.; Li, W.; Chen, X.; Yongsheng, L.; Qi, D. Heat dissipation optimization for a serpentine liquid cooling battery thermal management system: An application of surrogate assisted approach. *J. Energy Storage* **2021**, *40*, 102771. [[CrossRef](#)]
8. Jialin, L.; Gan, Y.; Li, Y. Investigation on the thermal performance of a battery thermal management system using heat pipe under different ambient temperatures. *Energy Convers. Manag.* **2018**, *155*, 1–9. [[CrossRef](#)]
9. Huang, M.; Eames, P.; Norton, B.; Hewitt, N. Natural convection in an internally finned phase change material heat sink for the thermal management of photovoltaics. *Sol. Energy Mater. Sol. Cells* **2011**, *95*, 1598–1603. [[CrossRef](#)]
10. Chen, J.; Kang, S.; E, J.; Huang, Z.; Wei, K.; Zhang, B.; Zhu, H.; Deng, Y.; Zhang, F.; Liao, G. Effects of different phase change material thermal management strategies on the cooling performance of the power lithium ion batteries: A review. *J. Power Sources* **2019**, *442*, 227228. [[CrossRef](#)]
11. Wu, W.; Liu, J.; Liu, M.; Rao, Z.; Deng, H.; Wang, Q.; Qi, X.; Wang, S. An innovative battery thermal management with thermally induced flexible phase change material. *Energy Convers. Manag.* **2020**, *221*, 113145. [[CrossRef](#)]
12. Landini, S.; Leworthy, J.; O'Donovan, T. A review of phase change materials for the thermal management and isothermalisation of lithium-ion cells. *J. Energy Storage* **2019**, *25*, 100887. [[CrossRef](#)]
13. Safdari, M.; Ahmadi, R.; Sadeghzadeh, S. Numerical investigation on PCM encapsulation shape used in the passive-active battery thermal management. *Energy* **2020**, *193*, 116840. [[CrossRef](#)]
14. Lin, C.; Xu, S.; Chang, G.; Liu, J. Experiment and simulation of a LiFePO₄ battery pack with a passive thermal management system using composite phase change material and graphite sheets. *J. Power Sources* **2015**, *275*, 742–749. [[CrossRef](#)]
15. Lazrak, A.; Fourmigue, J.; Robin, J. An innovative practical battery thermal management system based on phase change materials: Numerical and experimental investigations. *Appl. Therm. Eng.* **2018**, *128*, 20–32. [[CrossRef](#)]
16. Javani, N.; Dincer, I.; Naterer, G.; Rohrauer, G. Modeling of passive thermal management for electric vehicle battery packs with PCM between cells. *Appl. Therm. Eng.* **2014**, *73*, 307–316. [[CrossRef](#)]
17. Suo, Y.; Tang, C.; Jia, Q.; Zhao, W. Influence of PCM configuration and optimization of PCM proportion on the thermal management of a prismatic battery with a combined PCM and air cooling structure. *J. Energy Storage* **2024**, *80*, 110340. [[CrossRef](#)]
18. Dey, H.; Pati, S.; Randive, P.R.; Baranyi, L. Effect of finned networks on PCM based battery thermal management system for cylindrical Li-ion batteries. *Case Stud. Therm. Eng.* **2024**, *59*, 104572. [[CrossRef](#)]
19. Zhang, F.; Lu, F.; Liang, B.; Zhu, Y.; Gou, H.; Xiao, K.; He, Y. Thermal performance analysis of a new type of branch-fin enhanced battery thermal management PCM module. *Renew. Energy* **2023**, *206*, 1049–1063. [[CrossRef](#)]
20. Khaboshan, H.N.; Jalilantabar, F.; Abdullah, A.A.; Panchal, S. Improving the cooling performance of cylindrical lithium-ion battery using three passive methods in a battery thermal management system. *Appl. Therm. Eng.* **2023**, *227*, 120320. [[CrossRef](#)]
21. Sharma, D.K.; Agarwal, P.; Prabhakar, A. Effect of fin design and continuous cycling on thermal performance of PCM-HP hybrid BTMS for high ambient temperature applications. *J. Energy Storage* **2023**, *74*, 109360. [[CrossRef](#)]
22. Wang, W.; Zhang, X.; Xin, C.; Rao, Z. An experimental study on thermal management of lithium-ion battery packs using an improved passive method. *Appl. Therm. Eng.* **2018**, *134*, 163–170. [[CrossRef](#)]
23. Li, K.; Yao, X.; Li, Z.; Gao, T.; Zhang, W.; Liao, Z.; Ju, X.; Xu, C. Thermal management of Li-ion batteries with passive thermal regulators based on composite PCM materials. *J. Energy Storage* **2024**, *89*, 111661. [[CrossRef](#)]
24. Wu, W.; Ye, G.; Zhang, G.; Yang, X. Composite phase change material with room-temperature-flexibility for battery thermal management. *Chem. Eng. J.* **2022**, *428*, 131116. [[CrossRef](#)]
25. Luo, M.; Zhang, Y.; Wang, Z.; Niu, Y.; Lu, B.; Zhu, J.; Zhang, J.; Wang, K. Thermal performance enhancement with snowflake fins and liquid cooling in PCM-based battery thermal management system at high ambient temperature and high discharge rate. *J. Energy Storage* **2024**, *90*, 111754. [[CrossRef](#)]

26. Xie, N.; Zhang, Y.; Liu, X.; Luo, R.; Liu, Y.; Ma, C. Thermal performance and structural optimization of a hybrid thermal management system based on MHPA/PCM/liquid cooling for lithium-ion battery. *Appl. Therm. Eng.* **2023**, *235*, 121341. [[CrossRef](#)]
27. Chen, X.; Su, Y.; Zhang, Y.; Shen, J.; Xu, X.; Wang, X.; Zhou, F. Performance of thermal management system based on PCM/forked liquid-cold plate for 18650 cylindrical battery. *J. Energy Storage* **2024**, *91*, 112071. [[CrossRef](#)]
28. Zheng, J.; Chang, L.; Mu, M.; Li, J.; Li, C.; Ma, C.; Du, H. A novel thermal management system combining phase change material with wavy cold plate for lithium-ion battery pack under high ambient temperature and rapid discharging. *Appl. Therm. Eng.* **2024**, *245*, 122803. [[CrossRef](#)]
29. Shahid, S.; Agelin-Chaab, M. Experimental and numerical analysis of a hybrid cooling concept for an electric battery module. *Int. J. Heat Fluid Flow* **2024**, *106*, 109320. [[CrossRef](#)]
30. Shahid, S.; Agelin-Chaab, M. Investigation of thermal properties of phase change materials for novel hybrid thermal management strategies for cylindrical Li-ion cells. *Appl. Therm. Eng.* **2024**, *242*, 122471. [[CrossRef](#)]
31. Shahid, S.; Agelin-Chaab, M. Experimental and parametric analysis of a novel hybrid thermal management strategy for cylindrical lithium-ion cells. *Heat Transfer* **2024**, *53*, 2840–2863. [[CrossRef](#)]
32. Halliday, D.; Resnick, R.; Walker, J. *Fundamentals of Physics*, 12th ed.; John Wiley Sons: Hoboken, NJ, USA, 2012.
33. Peng, P.; Wang, Y.; Jiang, F. Numerical study of PCM thermal behavior of a novel PCM-heat pipe combined system for Li-ion battery thermal management. *Appl. Therm. Eng.* **2022**, *209*, 118293. [[CrossRef](#)]
34. Moffat, R.J. Describing the uncertainties in experimental results. *Exp. Therm. Fluid Sci.* **1988**, *1*, 3–17. [[CrossRef](#)]
35. Ganji, M.; Givian, M.; Gharali, K.; Ebadi, S.; Dastjerdi, S.M. Experimental optimization of partial metallic wire mesh configuration applicable in thermal energy storage systems. *Appl. Therm. Eng.* **2023**, *218*, 119274. [[CrossRef](#)]
36. Regin, A.F.; Solanki, S.C.; Saini, J.S. Heat transfer characteristics of thermal energy storage system using PCM capsules: A review. *Renew. Sustain. Energy Rev.* **2008**, *12*, 2438–2458. [[CrossRef](#)]
37. Moaveni, A.; Siavashi, M.; Mousavi, S. Passive and hybrid battery thermal management system by cooling flow control, employing nano-PCM, fins, and metal foam. *Energy* **2024**, *288*, 129809. [[CrossRef](#)]
38. Cengel, Y.A. Heat Transfer. In *Encyclopedia of Energy Engineering and Technology—Four Volume Set*; CRC Press: Boca Raton, FL, USA, 2014; pp. 846–853.

Disclaimer/Publisher’s Note: The statements, opinions and data contained in all publications are solely those of the individual author(s) and contributor(s) and not of MDPI and/or the editor(s). MDPI and/or the editor(s) disclaim responsibility for any injury to people or property resulting from any ideas, methods, instructions or products referred to in the content.